ERDHEIM CHESTER DISEASE: ROLE OF 18FDG PET/CT AND MORPHOLOGICAL IMAGING

Maseeh uz Zaman,[1] Nosheen Fatima,[1] Unaiza Zaman,[2] Farida Zafar Shakir[1]

[1] Section of NM and PET/CT Imaging, Department of Radiology, Aga Khan University Hospital, Karachi, Pakistan.

[2] Department of Hem Oncology, Oklahoma University, OK, USA.

PJR July - September 2024; 34(3): 149-156

Erdheim Chester disease (ECD) is a rare tumor of histiocytic origin which is characterized by presence of foamy / lipid laden histiocytes mixed or surrounded by fibrosis infiltrating multiple organs. Underdiagnosis or misdiagnosis is common due to diverse clinical presentations.[1] ECD is usually prevalent in middle-aged and older adults (median age: 55 year) with mild male predominance and central diabetes insipidus (CDI) in 25% to 50% of patients characterized by pituitary stalk enlargement on magnetic resonance imaging (MRI).[2] Furthermore, in >50% cases BRAF-V600E mutation is present.[2] BRAF-V600E mutations are associated with various malignancies like adenocarcinoma of lung, melanoma, thyroid papillary cancer and colorectal malignancies.[3] Therefore, ECD has been classified as a malignant disorder and presence of a BRAF-V600E mutation narrows the diagnosis toward ECD and LCH (Langerhans s cell histiocytosis) and excludes other types of histiocytosis.[4] Furthermore, presence of BRAF-V600E mutation also guides physician to use vemurafenib (targeted therapy) and use cladribine in BRAF-V600E negative patients.[1]

In recent years, diagnosis of ECD is on rise and till 2024, more than 1500 cases of ECD have been reported in literature.[1] Early diagnosis of ECD is challenging due to its broad and nonspecific clinical presentation, low prevalence, inconsistent pathological findings, and lack of clinician awareness of the disease. The purpose of this mini review related to a recently diagnosed case of ECD is to provide clinicians reading 18FDG PET/CT with a resource to facilitate diagnosis of ECD and treatment response assessment using follow-up studies. Median survival from the initial onset of ECD is about 10 years, in most cases being progressive and fatal within a few years.[4]

Case Report

A 44-yearmale, non-diabetic and normotensive presented with chronic folliculitis in left axilla and short history of mild left eye proptosis. In 2020, he had a biopsy of retroperitoneum which revealed scattered foamy microphages and mild chronic inflammation (no specific diagnosis could be made). His previous medical history is also significant for the treatment of tuberculosis. He was clinically investigated with provisional diagnosis of lymphoma or autoimmune disorder.

His complete blood picture (CBC) revealed thrombocytosis (538 x 10E9/L; Normal: 154 -433) and routine biochemistry revealed raised alkaline phosphatase (365 IU/L; Normal: 40-129). Antinuclear antibody test (ANA) was positive while extra-nuclear antigen panel (ENAP), anti-DNA, ANCA, ASMA and AMA were negative. His serum angiotensin converting enzyme (ACE) and IgG4 levels (1010 mg/l; normal: 30-2010) were within normal limits. His contrast enhanced computerized tomography (CECT) revealed enhancing soft tissue lesions encasing left optic nerve (29 x 25 mm) with proptosis and a smaller in right orbit along right optic nerve (12 x 9 mm) without proptosis and normal appearing both globes,

Correspondence : Dr. Maseeh uz Zaman
Section of NM and PET/CT Imaging,
Department of Radiology, Aga Khan University Hospital,
Karachi, Pakistan.
Email: maseeh.uzzaman@aku.edu

Submitted 21 August 2024, Accepted 26 August 2024

extraocular muscles and optic nerves. Minimal bone remodeling without erosion was also seen in left orbit but no abnormality was noted in brain. Magnetic resonance imaging (MRI) brain with contrast redemonstrated soft tissue intraconal lesions in both orbits encasing optic nerves (left: 22 x 31 x 21 mm; Right 09 x 14 x 06 mm) with essentially normal brain parenchyma with differential of lymphoma or IgG4 related disease. This was followed by ^{18}FDG PET/CT (Fluorodeoxyglucose positron emission tomography/ computerized tomography) and which revealed hypermetabolic (enhanced ^{18}FDG avid) soft tissue lesion encasing left optic nerve with mild proptosis but non-avid subcentimeter right orbital lesion (likely due to partial volume effect), hypermetabolic soft tissue thickening in left axilla (site of clinically known infection) and non-homogenous ^{18}FDG uptake over right atrium and significant bilateral peri-nephric fat stranding. Rest of the PET/CT examination was unremarkable. A follow-up echocardiogram was within normal limits. Finally, biopsy of left orbital lesion revealed fibroadipose tissue with sheets of foamy macrophages and mild inflammatory infiltrates favouring Erdheim-Chester disease. His previous retroperitoneal biopsy performed in 2020, was also reviewed which revealed similar features, but ECD was not concluded in that report. Immunohistochemistry panel also favour Erdheim-Chester disease, not featuring clearcut Rosai-Dorfman component without remarkable IgG4 reaction. Mutation testing using Erlanger QIAGEN NGS panel revealed BRAF-V600E mutation with low allele frequency of 5% characteristic of ECD due to extensive reactive / inflammatory component.

Erdheim-Chester Disease presentations on morphological and metabolic imaging.

Histology and genetic mutation: ECD is a systemic non-Langerhans histiocytosis with a wide range of findings from asymptomatic sclerotic bony lesions to life-threatening involvement of vascular and retroperitoneal structures. Histologically, ECD has xanthomatous features, fibrosis, and occasional Touton giant cells. ECD histiocytes stain positive for CD68 and negative for CD1a, langerin, and S100 (rarely ECD can stain faintly positive for S100).[5] Presence of BRAF-V600E mutations (in >50% cases) is associated with various malignancies as described above and guides for selecting an appropriate therapeutic agent for better disease outcome.[1]

Clinical Presentation and Imaging: The diagnosis of ECD is challenging due to rarity and varied presenting sign and symptoms. Common symptoms include dyspnea, bone pain, ataxia, and visual disturbance.[5] Sclerotic bony lesions are almost universally present inmorphological imaging but only 50% of patients have symptoms for bone pain.[6] Imaging plays a key role in diagnosing ECD. Morphological imaging modalities like plain radiography, CT and MRI have been used for focused evaluation but lack the accuracy for assessing the disease burden / severity and assessment of response to treatment. In contrast, hybrid imaging like ^{18}FDG PET/CT has been found of pivotal value for diagnosis by revealing the extent of multi-system involvement and by identifying potential biopsy sites and presence of metabolic activity is associated with BRAF-V600E mutationin >50% cases.[2,7] In addition, accumulating evidence suggests efficacy of ^{18}FDG PET/CT scan in disease follow-up, therapy selection, response evaluation and restaging as well.

Skeletal System: In majority of ECD cases bones are involved, predominantly long bones around knees (dia-metaphyseal mainly) and less commonly axial skeleton. In this patient, plain radiography was performed in 2017 due to painful left knee, revealed irregularity with increased cortical density particularly on the posterior aspect. Medullary region also showed slightly increased density in the distal part of left femur and proximal tibia (Fig.1).

Figure 1: Plain radiographs (**A:** AP view; **B:** Lateral view) of left knee showing increased sclerosis and irregularity particularly on the posterior aspect of tibia andmedullary region of visualized left femur and tibia.

MRI of left knee performed in 2017 revealed diffuse-altered marrow signals with geographical distribution in distal femur and proximal tibia with relative endosteal sclerosis in distal femur. There was no bony erosion, preserved joint cavity with mild effusion (Fig.2).

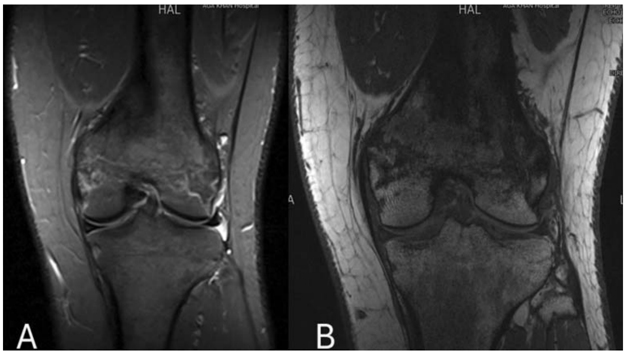

Figure 2: MRI of left knee (**A:** T1 weighted; **B:** T2 weighted) images showing diffuse abnormal marrow signals in distal femur and proximal tibia with a geographical pattern, sclerosis in distal shaft of femur without bony erosion.

Skeletal lesions are usually metabolically active ^{18}FDG PET/CT with underlying sclerosis. However, in our case visualized skeleton (head to mid-thigh) did not show sclerotic or metabolically active lesions but unfortunately distal appendicular skeleton was not in field of view (Fig.3). Therefore, this limitation supports the use of vertex to toe (total body) protocol for ^{18}FDG PET/CT in patients with suspected ECD. However,

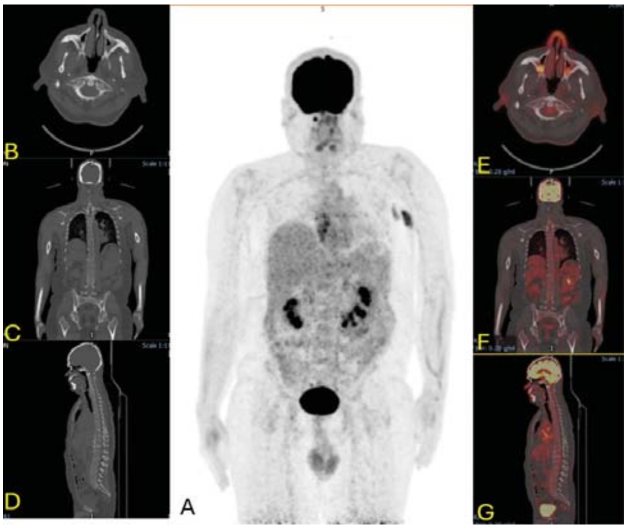

Figure 3: ^{18}FDG PET/CT (Head to mid-thigh) performed in 7/2024; **(A)** maximum intensity projection image (MIP) showing intense metabolic activity in left axilla consistent with clinically known cellulitis. **(B-G)** bone window show sparing of visualized axial and proximal appendicular skeleton and supports the use of vertex to toe (total body) protocol for ^{18}FDG PET/CT in patients with suspected ECD.

^{18}FDG uptake may occur prior the appearance of osteosclerosis (Fig.4).[7]

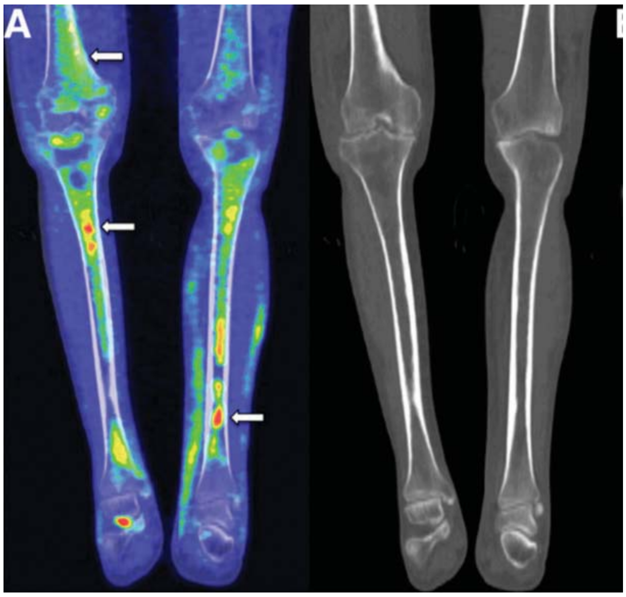

Figure 4: Coronal ^{18}FDG PET/CT of distal lower extremities demonstrates hypermetabolic marrow disease within both tibias and distal femur (arrows) without osteosclerosis *(Adopted with kind permission by Dr Stephen M. Broski, Mayo Clinic, Rochester, MN)*.

Kidneys: Involvement of kidneys is also common in ECD and reported incidence is about 80%.[9] Histiocytes frequently infiltrate the peri-nephric space, renal pelvis and proximal ureters leading to obstructive uropathy. CT KUB (Kidney, ureter, bladder) performed in this patient in 2020 also revealed swollen bilateral kidneys with significant perinephric and periureteric fat stranding and thickening of the Gerota's fascia (hairy kidneys) with preserved corticomedullary differentiation. There is fullness of bilateral pelvicalyceal system with non-obstructing bilateral calculi (Fig.5).

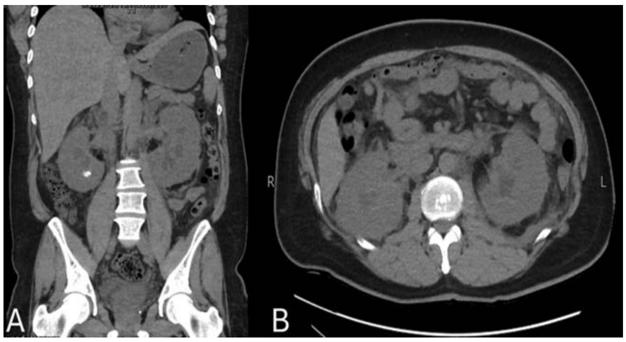

Figure 5: CT KUB (coronal **[A]** and axial **[B]**) images showing swollen hairy kidneys with significant fat stranding and thickening of Gerota fascia and stone in right kidney.

In addition to hairy kidneys presentation on CT, other manifestationsin ECD are poor corticomedullary differentiation (featureless kidney), and a rim of cortical calcification (goose egg kidneys) (Fig.6).

Figure 6: CT KUB coronal image shows interrupted rim of calcification in both kidneys (arrow) with perinephric fat stranding (hairy kidney*) [*Adopted with kind permission by Dr Stephen M. Broski, Mayo Clinic, Rochester, MN*].

[18]FDG PET/CT images in 2024, redemonstrated bilateral perinephric fat stranding, thickness of Gerota fascia, bilateral calculi with reduction in size of right but increase of left kidneys (Fig.7).

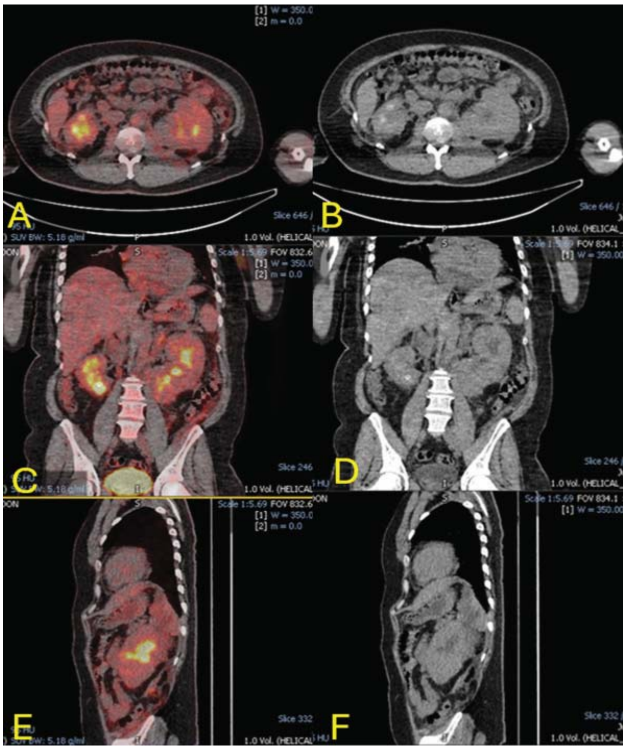

Figure 7: [18]FDG PET/CT study (**A,C,E:** fused axial, coronal and sagittal views; **B,D,F:** unenhanced CT axial, coronal and sagittal views) showing enlarged left kidney, bilateral hydronephrosis, right renal stones and perinephric fat stranding and thickened Gerota fascia (hairy kidneys).

Central Nervous System (CNS): Is considered the 3rd most common site of involvement and leads to substantial morbidity and mortality.[7] CNS manifestation is usually determined by clinical examination and MRI of brain and spine. In a recently published French study, CNS involvement was seen in 38% of cohort, predominantly at a younger age (around 55 Yr) and a strong association with BRAF-V600E mutation (77%).[10] Three distinct patterns can be recognized: tumoral, pseudo-degenerative, and vascular.[10] ECD could involve the cerebrum, cerebellum, pons, and spinal cord. Extra-axial disease may also present as thick plaque like soft tissue, layered along dural membranes (Fig.8). However, in our patient, CNS was spared as evident on MRI study.

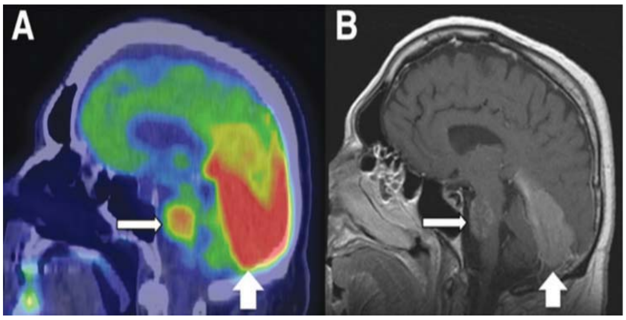

Figure 8: 50-y-old man with left mastoid pain. **(A)** Sagittal fused PET/CT demonstrates [18]FDG-avid disease within pons (thin white arrow) and along tentorium (thick white arrow). **(B)** Corresponding contrast-enhanced MRI illustrates infiltrative pons lesion (thin white arrow) and enhancing soft-tissue thickening along tentorium (thick white arrow) [*Adopted with kind permission by Dr Stephen M. Broski, Mayo Clinic, Rochester, MN*].

Paranasal Sinuses: Involvement of paranasal sinuses by ECD is also common and predominantly involve maxillary sinuses. In a reported study, paranasal sinuses infiltration was seen particularly for maxillary and sphenoid sinuses (47%) as opposed to the involvement of ethmoidal and frontal sinuses (17%).[11] PET/CT may reveal hypermetabolism of the sinuses, an element supporting ECD diagnosis. Some studies have reported a close association between sinus involvement with BRAF-V600E mutation as well.[12] Presentation varies from mild [18]FDG avid mucosal thickening without bony abnormality to hypermetabolic mucosal thickening with underlying osteosclerosis. In our patient, there was hypermetabolic mucosal thickening without bony abnormality in bilateral maxillary sinuses (predominantly on right; Fig.9).

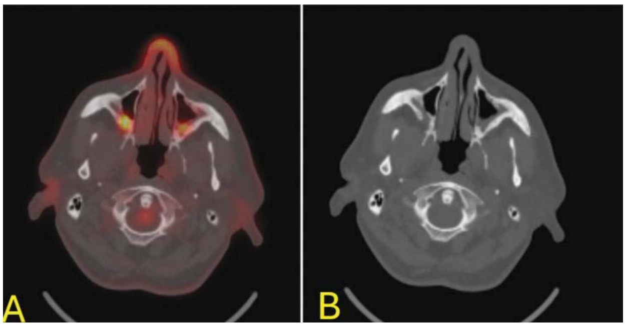

Figure 9: Axial fused **(A)** and non-enhanced CT **(B)** images showing focal hypermetabolic mucosal thickening over posterior aspect of bilaterally maxillary sinuses without osteosclerosis (more on right).

Orbital Disease: Is reported in 38% of patients in one case series.[7] Usual presentation is soft tissue thickening of variable volume encasing bilateral optic nerveson CT and MRI with mild to moderate [18]FDG avidity on PET/CT and proptosis. Incidence of involvement of globes by ECD is less common but reportedly may involve sclera and choroid. Our patient was presented with left sided mild proptosis with presence of soft tissue abnormality on MRI (Fig.10), CT (Fig.11) and [18]FDG PET/CT (SUVmax 5.7; Fig.12). Biopsy of left sided lesion was positive for ECD.

Cardio-vascular involvement: In ECD, non-Langerhans histiocyte infiltration inflicting the heart has been reported in 40% to 75% of cases and mortality may reach up to 60% in 32 months, particularly when there is cardiac involvement.[13] On cardiac MRI, ECD

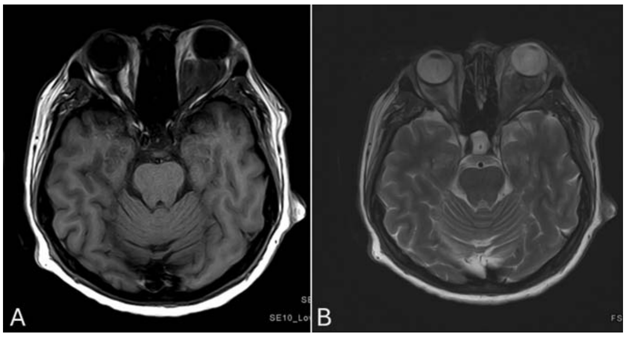

Figure 10: MRI axial images (**A:** T1-weighted; **B:** T2-weighted) showing an enhancing left intraconal lesion encasing the left optic nerve (22 x 31 x 21 mm) and a smaller right intraconal lesion partially encasing the right optic nerve (9 x 14 x 6 mm). Nonspecific enhancement of bilateral medial and lateral pterygoid muscles could bedue to inflammation or infiltrative process.

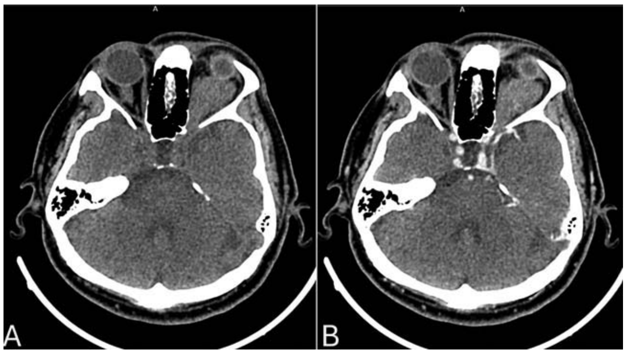

Figure 11: CT brain axial slices without **(A)** and with contrast **(B)** showing enhancing, lobulated bilateral retro orbital lesions (Left: 29 x 25 mm; Right: 12 x 9 mm) with minimal bony remodeling without erosion on left side.

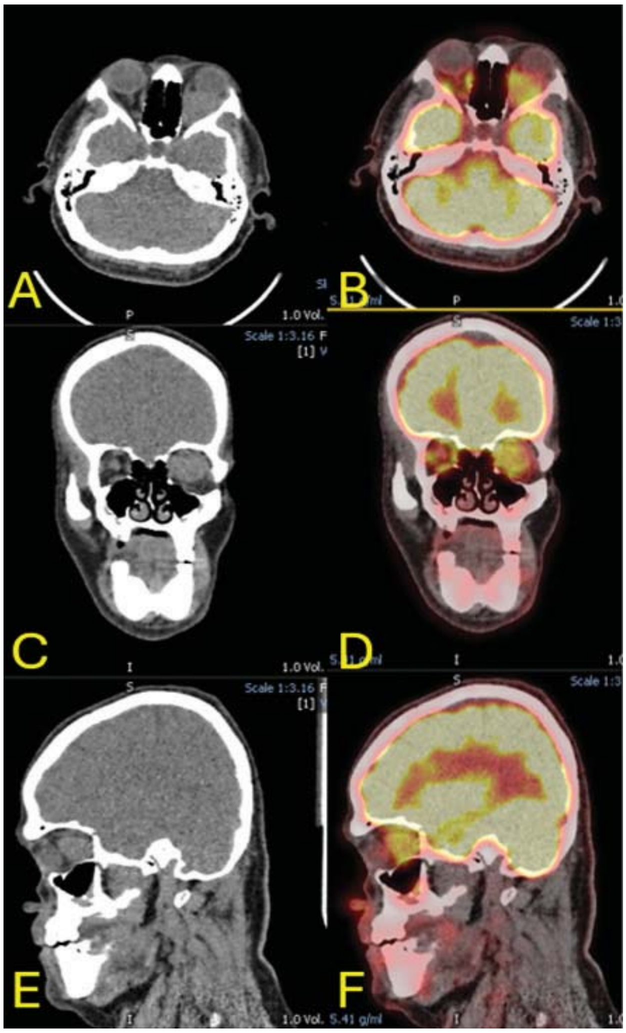

Figure 12: Non-enhanced low dose [18]FDG PET/CT study (**A, B:** axial; **C, D:** coronal; **E, F:** sagittal) showing mild [18]FDG avid soft tissue mass in left orbit behind globe encasing left optic nerve (32 x 21 mm; SUVmax 5.7). The right orbital lesion did not show metabolic activity likely due to partial volume effect due to its smaller size.

involvement is characterized by infiltration with hypointense signal within the atrioventricular groove surrounding the right coronary artery, right atrium walls, interatrial septum (sparing the fossa ovalis), and periadventitial region of descending aorta and diffuse fibrosis with late gadolinium enhancements.[14]

On ^{18}FDG PET/CT common presentation is metabolic activity soft tissue thickening involving adventitia and myocardium and pericardium with reported predilection for right atrium.[15] Our patient has shown moderate ^{18}FDG avidity over base of heart, predominantly over right atrium (SUVmax 7.3; Fig.13). Follow-up echocardiogram was negative for any vegetation, but no cardiac MRI was done. In our case, there was no morphological or metabolic evidence of aortic involvement on ^{18}FDG PET/CT. However, a reported case has revealed peri-aortic ^{18}FDG avid soft coating due to involvement of tunica adventitia - coated aorta (Fig.14).[7]

Peritoneal, mesentry and retroperitoneal disease: Is reported in 34% of cases in a large series.[7] Mild to moderate ^{18}FDG lesions involving these sites are seen. Our patient has had retroperitoneal fibrosis with

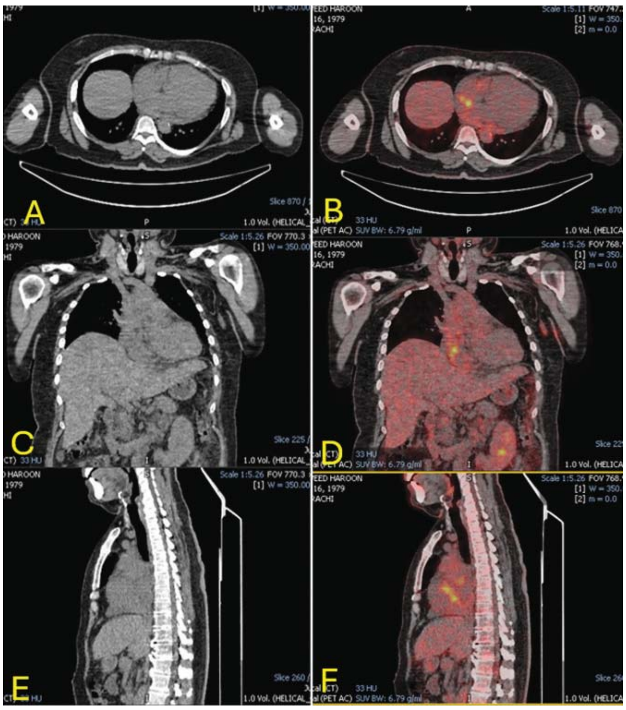

Figure 13: Low dose non-enhanced ^{18}FDG PET/CT (**A,C,E:** non-enhanced axial, coronal and sagittal; **B,D,F:** fused axial, coronal and sagittal) shows linear shaped enhanced non-homogenous metabolic activity over right atrium (SUVmax 7.3).

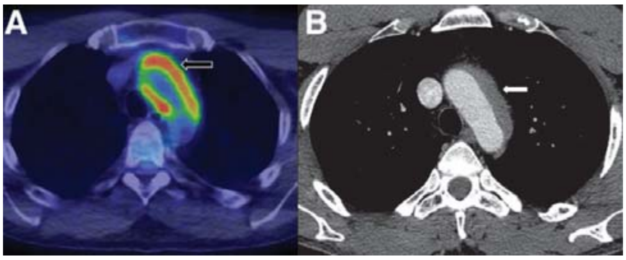

Figure 14: A: Axial fused demonstrate intensely hypermetabolic softtissue thickening around aortic arch (arrow); **B:** (CECT) demonstrates soft tissue along the outer wall of aortic arch (coated aorta; arrow). [*Adopted with kind permission by Dr. Stephen M. Broski, Mayo Clinic, Rochester, MN*].

involvement of uretres, swollen kidneys with stones, thickenend fascia of Gerota and diffuse omental / mesetric nodularity (Fig.15). This was redemonstrated in recent ^{18}FDG PET/CT imaging as shown in (Fig.6).

Figure 15: Non-enhnaced CT KUB (**A:** Coronal; **B:** axila at proximal renal; **C:** axial at mid renal level) showing significant perinephric fat straning, thickened facsia of Gerota and peritoneal fuzziness.

Nodal Disease: Involvement of nodes is rare in ECD in contrast to Rosai-Dorfman disease which is characterized by reactive histiocytic proliferation occurring mainly in lymph nodes.[16] In this case we also could not discern any nodal involvement and similarly in a case series only only 2/32 cases revealed mild ^{18}FDG uptake in thoracic nodes which were condiered reactive by authors.[7]

BRAF-V600E Mutation: This mutation accounts for about 50% of the cases and is associated with various malignancies like adenocarcinoma of lung, papillary carcinoma of thyroid, colorectal Ca and melanoma.[3] For this reason, ECD has been classified as a malignant disorder and narrows the diagnosis toward ECD and LCH, excluding all other types of histiocytosis.[4,17] According to one study, presence of a BRAF mutation was significantly associated with ^{18}FDG-avid CNS disease, higher SUVmax and higher mortality and act as a biomarker for presence of this mutation.[7] The presence of BRAF-V600E mutation also guides the physicians to use vemurafenib (targeted therapy, approved by Food and Drug Administration (FDA) and cladribine in patients not having mutation. Our patient also has BRAF-V600E mutation and follow-up ^{18}FDG PET/CT will be used for metabolic response assessment.

Diagnosis of ECD is challenging and imaging plays a key role in diagnosis. In recent years, ^{18}FDG PET/CT has emerged from imaging armamentarium comprised of other morphological imaging modalities. It is due to its hybrid and whole-body coverage, guiding the most ^{18}FDG avid site for biopsy, strong correlation with BRF-V600E mutation, treatment selection and metabolic response assessment.

Conflict of Interest: None.

References

1. Shi X, Sun G, Li T, Xu M, Liu Y, Wang Z, et al. Erdheim Chester disease of multisystem involvement with delayed diagnosis: A case report and literature review. Exp Ther Med. Feb 2024; **27(4):** 159.

2. Khoury JD, Solary E, Abla O, Akkari Y, Alaggio R, Apperley JF, et al. The 5th edition of the World Health Organization Classification of Haematolymphoid Tumours: Myeloid and histiocytic/dendritic neoplasms. Leukemia. 2022; **36:** 1703-19.

3. Cui G, Liu D, Li W, Xiao Fu, Youguang Liang, Yuhang Li, et al. A meta-analysis of the association between BRAF mutation and nonsmall cell lung cancer. Medicine (Baltimore). 2017; **96:** e6552.

4. Haroche J, Charlotte F, Arnaud L, Deimling A, Zofia HR, Hervier B, et al. High prevalence of BRAF V600E mutations in Erdheim-Chester disease but not in other non-Langerhans cell histiocytoses. Blood. 2012; **120:** 2700-3.

5. Diamond EL, Dagna L, Hyman DM, Cavalli G, Janku F, Estrada-VerasetJ, et al. Consensus guidelines for the diagnosis and clinical management of Erdheim-Chester disease. Blood. 2014; **124:** 483-92.

6. Haroche J, Arnaud L, Cohen-Aubart F, Hervier B, Charlotte F, Emileet JF, et al. Erdheim-Chester disease. Curr Rheumatol Rep. 2014; **16:** 412.

7. Jason R. Young, Geoffrey B. Johnson, Robert C. Murphy, Ronald S. Go, Stephen M. Broski. 18F-FDG PET/CT in Erdheim-Chester Disease: Imaging Findings and Potential BRAF Mutation Biomarker. J Nucl Med 2018; **59:** 774-9.

8. White TV, Silvester NC, Otero HJ. Non-sclerotic bone involvement in ErdheimChester: PET/CT and MRI findings in a 15-year-old boy. Pediatr Radiol. 2016; **46:** 1345-9.

9. Ganiyusufoglu AK, G ksenoglu G, Tun B, Paker N. Erdheim-Chester Disease With Renal Involvement: A Case Report. Arch Rheumatol. Feb 2017; **32(2):** 167-70.

10. Cohen Aubart F, Idbaih A, Galanaud D, Law-Ye B, Emile JF, Charlotte F, Donadieu J, Maksud P, Seilhean D, Amoura Z, Hoang-Xuan K, Haroche J. Central nervous system involvement in Erdheim-Chester disease: An observational cohort study. Neurology. Nov 2020; **95(20):** e2746-e2754.

11. Haroche J, Cohen-Aubart F, Amoura Z. Erdheim-Chester disease. Blood. Apr 2020; **135(16):** 1311-8.

12. Drouillard M, Trunet S, Hervochon R, Azoulay LD, Amoura Z, CohenAubart F, et al. Sinonasal and ear manifestations of Erdheim-Chester disease. Br J Haematol. 2023; **203:** 194-201.

13. Ponsiglione, A, Puglia, M, Barbuto, L, Solla, R, Altiero, M, Lubrano, V, Imbriaco, M. Cardiac involve-

ment in Erdheim- Chester disease: MRI findings and literature revision. Acta Radiol Open. 2015; **4:** 2058460115592273.

14. Quinaglia-Silva T, Medina F, Ramos CD, Coelho-Filho OR. Cardiac Involvement in Erdheim-Chester Disease. Circ Cardiovasc Imaging. Dec 2018; **11(12):** e008531.

15. Haroche J, Cluzel P, Toledano D, Montalescot G, Touitou D, Grenier PA,et al. Images in cardio-vascular medicine: cardiac involvement in Erdheim-Chester disease-magnetic resonance and computed tomographic scan imaging in a monocentric series of 37 patients. Circulation. 2009; **119:** e597-e598.

16. B sm ller H, Nann D, Horger M, Fend F. Erdheim-Chester disease and RosaiDorfman disease: pathological, radiological and clinical features of adult nonLangerhans cell histiocytosis [in German]. Pathologe. 2015; **36:** 458-66.

17. Swerdlow SH, Campo E, Pileri SA, Harris NE, Stein H, SiebertetR, et al. The 2016 revision of the World Health Organization classification of lymphoid neoplasms. Blood. 2016; **127:** 2375-90.